Naval Research Laboratory

Washington, DC 20375-5320

NRL/MR/6410--08-9132

Regular and Mach Reflections to Mach 18 with Air and TNT Detonation Products

DOUGLAS SCHWER

Center for Reactive Flow and Dynamical Systems
Laboratory for Computational Physics and Fluid Dynamics

September 10, 2008

REPORT DOCUMENTATION PAGE

Form Approved
OMB No. 0704-0188

1. REPORT DATE *(DD-MM-YYYY)*	**2. REPORT TYPE**	**3. DATES COVERED** *(From - To)*
10-09-2008	Memorandum Report	

4. TITLE AND SUBTITLE

Regular and Mach Reflections to Mach 18 with Air and TNT Detonation Products

5a. CONTRACT NUMBER

5b. GRANT NUMBER
64-1530-1-7

5c. PROGRAM ELEMENT NUMBER

6. AUTHOR(S)

Douglas Schwer

5d. PROJECT NUMBER

5e. TASK NUMBER

5f. WORK UNIT NUMBER

7. PERFORMING ORGANIZATION NAME(S) AND ADDRESS(ES)

Naval Research Laboratory, Code 6410
4555 Overlook Avenue, SW
Washington, DC 20375-5320

8. PERFORMING ORGANIZATION REPORT NUMBER

NRL/MR/6410--08-9132

9. SPONSORING / MONITORING AGENCY NAME(S) AND ADDRESS(ES)

Office of Naval Research
One Liberty Center
875 North Randolph Street
Arlington, VA 22203-1995

10. SPONSOR / MONITOR'S ACRONYM(S)

ONR

11. SPONSOR / MONITOR'S REPORT NUMBER(S)

12. DISTRIBUTION / AVAILABILITY STATEMENT

Approved for public release; distribution is unlimited

13. SUPPLEMENTARY NOTES

14. ABSTRACT

This report describes the computation of critical incident shock wave angles for regular (α_N) and Mach (α_d) reflections as a function of Mach number up to 18. First, the effect of different values for the specific heat ratio (γ) is examined, and is found that as γ decreases from 1.4 to 1.2, the value for α_N decreases for regular reflections, and the value for α_d increases, resulting in a significantly larger dual-solution-domain. Next, temperature dependent properties for air were used with standard temperature and pressure inflow conditions. These results were compared with the perfect gas case with γ set to 1.4, and showed that the variable properties calculation had very little effect on the α_N value. However, variable properties had a significant effect on the α_d value, because Mach reflections represent stronger shock waves with larger temperature jumps across the shock wave. The next set of results compared the air with variable properties results with results using variable properties and TNT detonation products. Again, we found that the α_N followed the perfect gas case closely with γ set to 1.2, while the α_d value differed substantially from the perfect gas and variable air properties cases. All cases were significantly different from the $\gamma = 1.4$ case. Finally, results were computed for air with variable properties and equilibrium chemistry. We found that α_N was not sensitive to equilibrium chemistry over the entire range of Mach numbers while α_d increased significantly at the higher Mach numbers. At Mach 18, the values for α_N varied between 18.9° (detonation products) and 23.1° ($\gamma + 1.4$), and the values for α_d varied between 39.9° ($\gamma = 1.4$) and 49.2° (detonation products). In general, we found α_N to be fairly insensitive to variable specific heats even at very high Mach number inflow, and adequate approximations can be made without considering variable specific heat or equilibrium reactions, although careful attention should be made to the selection of γ. α_d, however, is very sensitive to both variable specific heats and quilibrium chemistry, and both should be considered when computing this critical value above Mach 5.

15. SUBJECT TERMS

Oblique shock waves | Regular reflections | Variable properties
Mach reflections | Detonation products | Chemical equilibrium

16. SECURITY CLASSIFICATION OF:			**17. LIMITATION OF ABSTRACT**	**18. NUMBER OF PAGES**	**19a. NAME OF RESPONSIBLE PERSON**
a. REPORT	**b. ABSTRACT**	**c. THIS PAGE**			Douglas Schwer
Unclassified	Unclassified	Unclassified	UL	13	**19b. TELEPHONE NUMBER** *(include area code)* (202) 767-3615

Introduction

This report details work on applying real gas properties to the determination of critical values of shock wave angle for regular reflections (α_N) and Mach reflections (α_d). An excellent review of regular and Mach reflections has been given in Hornung [1], which describes the physical process. More recent work has been done with respect to numerical simulations in the dual-solution-domain [2], where either regular or Mach reflections can exist. Most of the work to date has, however, focused on relatively weak shock waves and perfect gas, constant-γ shock wave processes. The purpose of the current research is to extend these results to Mach numbers up to 18, where variable properties and reactions can be important.

There are two main effects when considering high Mach number flows with strong shock waves. The first effect of importance is a variable specific heat. As higher temperatures are achieved behind the shock, the specific heat for molecules will typically increase as vibrational and eventually electronic states become excited in the molecules, shifting the specific heat ratio towards one and effecting the shock wave. The second main effect is reactions. Reactions can occur behind the shock due to combustion or dissociation, which either add or remove heat from the gas behind the shock wave. For this report we focus on dissociation, and use an equilibrium calculation to determine the shocked gas composition.

Problem Statement

The problem of interest is illustrated in Figure 1. Flow enters the domain at a given temperature, pressure, mole-fractions, and velocity. For the cases described here, the inflow pressure and temperature are one atm and 298.15 K. The flow encounters a wedge, which creates an oblique shock wave (we only consider angles producing oblique, attached shock waves). This shock wave is then reflected off of the top wall or symmetry plane. Two types of reflections can occur, dependent on the inflow conditions and the wedge angle. The first type of reflection is a regular reflection, where an oblique shock wave is reflected off of the surface. The second type is a Mach reflection, where the incident shock transitions to a normal shock near the top wall or reflected boundary. For inflow Mach numbers greater than 2.2, there are two critical values for the wedge angle (and thus shock wave angle) that determine the type of reflection that occurs. For $\alpha < \alpha_N$ only regular reflections occur, and for $\alpha > \alpha_d$ only Mach reflections occur. However, for $\alpha_N < \alpha < \alpha_d$ both regular and Mach reflections occur. This region is known as the dual-solution-domain (DSD). Both critical values for α are found by considering the regular reflection case.

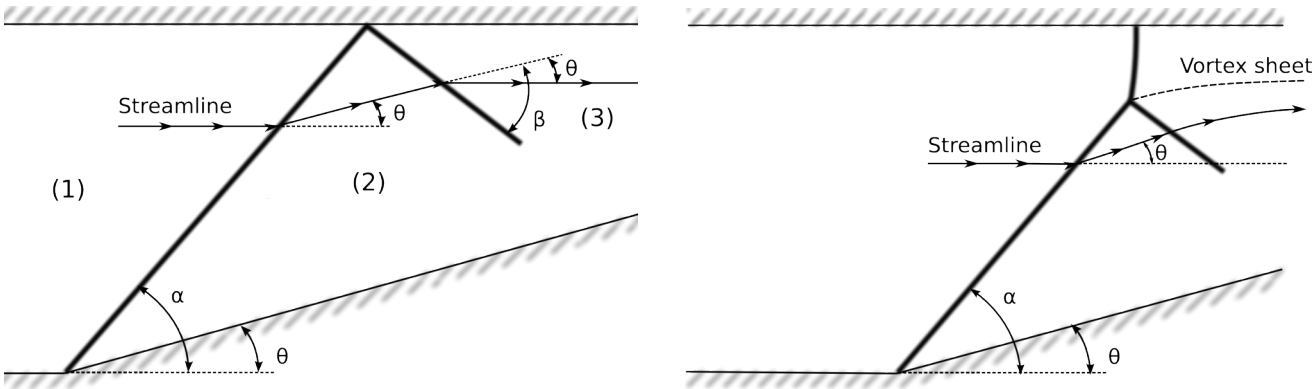

Figure 1. Schematic of regular reflection (left) and Mach reflection (right) off of a solid wall boundary.

Manuscript approved June 3, 2008.

For regular reflections, the analysis is divided into two oblique shock wave solutions. Conditions ahead of the incident shock wave are described as condition (1), and behind the incident shock wave we have condition (2). These conditions serve as the pre-shock conditions for the reflected shock wave calculation. The flow after the reflected shock wave is represented as condition (3). The next section details the solution method used for oblique shock waves.

Oblique Shock Wave Analysis

The oblique shock-wave solution is found by applying the appropriate mass, momentum, and energy conservation equations along with an equation of state and thermodynamic relations. For an oblique shock-wave, we first identify the component of velocity normal to the shock-wave (u) and the component of velocity tangential to the shock-wave (w). Labeling pre-shocked properties with a subscript 1 and shocked properties with a subscript 2, we can develop conservation equations for the shocked gases after an oblique shock-wave. For a shock wave angle of α, the velocity components are

$$u_1 = V_1 \sin\alpha \tag{1}$$

$$w_1 = V_1 \cos\alpha \tag{2}$$

where V_1 is the initial velocity of the flow. Conservation of mass, momentum, and energy reduces to:

$$\rho_1 u_1 = \rho_2 u_2 \tag{3}$$

$$w_1 = w_2 \tag{4}$$

$$p_1 + \rho_1 u_1^2 = p_2 + \rho_2 u_2^2 \tag{5}$$

$$h_1 + \frac{u_1^2}{2} = h_2 + \frac{u_2^2}{2} \tag{6}$$

In addition, we have auxiliary equations in the form of the equation of state and thermodynamic relations to close the system of equations. This can be summarized as:

$$\rho_2 = \rho\left(p_2, h_2\right) \tag{7}$$

After computing the shocked gas properties, we can calculate the deflection angle as

$$\theta = \alpha - \tan^{-1}\frac{u_2}{w_2} \tag{8}$$

where θ is the deflection angle. For a perfect gas with a constant γ, the above relations can be reduced to two independent variables, M_1 and α. Pressure and temperature ratio, and Mach number are all expressed as functions of M_1 and γ. For real gases with possible reactions, this is no longer possible, and the resultant pressure and temperature ratios are dependent on the pre-shocked pressure, temperature, velocity, and mixture composition. To solve this system, we need to know enthalpy and specific heat as a function of temperature and pressure. For the equilibrium reaction computations, we also need to determine mixture composition as a function of pressure and enthalpy. Appendix A gives more details on the iterative solution to the conservation equations, Appendix B describes how the thermal properties of the gas are computed, and Appendix C describes how the equilibrium composition of the gas is found.

Deflection Diagrams

The preceding equations represent the core computations for our problem of interest. For our problem, we are interested in understanding how the pressure ratio (p/p_1) and deflection angle (θ) vary as the incident angle varies (α). As mentioned previously, for a perfect gas with no reactions, these variables are dependent solely on the upstream Mach number. However, for variable specific heats and reactions, this problem is dependent on all of the inflow conditions, $u_1, P_1, T_1, X_{1,i} = \mathbf{C}_{(1)}$. In the computations completed in this report, the upstream pressure and temperature are one atm and 298.15 K, and the mole-fractions are specified as either air or detonation products. We still report the findings in terms of the upstream Mach number, to provide comparisons with previous work with constant specific heat ratios. Note, however, that if the inflow temperature, pressure, or mole-fractions are altered, the curves presented will also shift.

The minimum incident angle that will produce a shock-wave is based on the requirement that the velocity normal to the shock-wave must at least be sonic. This reduces to the equation:

$$\alpha_{min} = \sin^{-1}\frac{1}{M_1} \tag{9}$$

α is then varied between α_{min} and $\pi/2$, which represents a normal shock. Solving the oblique shock relations as α varies between α_{min} and $\pi/2$ gives us deflection-pressure diagrams. In Figure 2, we consider inflow air at standard temperature and pressure and a velocity corresponding to Mach 3. The independent variable to produce this plot is the incident angle, α, and the reflected angle, β, even though the horizontal axis for these plots is the deflection angle, θ.

An important characteristic of pressure-deflection diagrams is that we can represent the entire incident-reflected shock-wave phenomenon on one plot. We simply superimpose both pressure-deflection diagrams on the same plot, translating the reflected shock-wave diagram to the correct initial pressure and deflection angle. The pressure-deflection diagram in Figure 2 represents the shock-wave pattern illustrated in Figure 1. Conditions at location (3) are found by determining where the pressure-deflection diagram for the reflected shock-wave intersects the vertical axis. Note that each deflection angle represents two unique values for pressure and also for shock wave angle, α, and that for any given Mach number, there is a maximum deflection angle for which an attached oblique shock-wave can exist. More details for deflection-pressure diagrams is given in the review article [1].

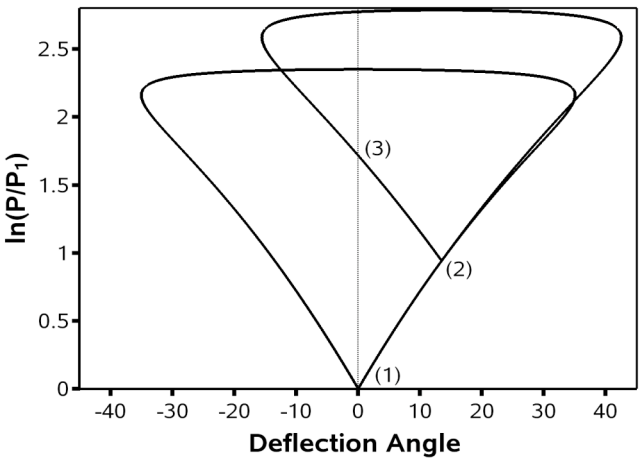

Figure 2. Pressure-deflection diagram for incident and reflected shock. Upstream condition is air at standard temperature and pressure, and the Mach number of the flow is 3 and γ=1.4.

In a like manner, we can show a series of deflection-pressure diagrams for the same inflow conditions (1), but differing deflection angles θ. This is shown in Figure 3 for two different Mach numbers, Mach 3 and 8. There are a some important things to note in Figure 3. First, as the deflection angle increases (and thus the shock wave angle α increases), the incident shock wave becomes stronger, and the reflected shock wave becomes weaker due to the lower Mach number in region (2). This results in a smaller deflection-pressure curve for the reflected shock wave, as can be seen in the Figure. There are two critical values for α that are labeled in the Figure. The first critical value, labeled α_N, is where the pressure at location (3) equals the normal shock pressure for

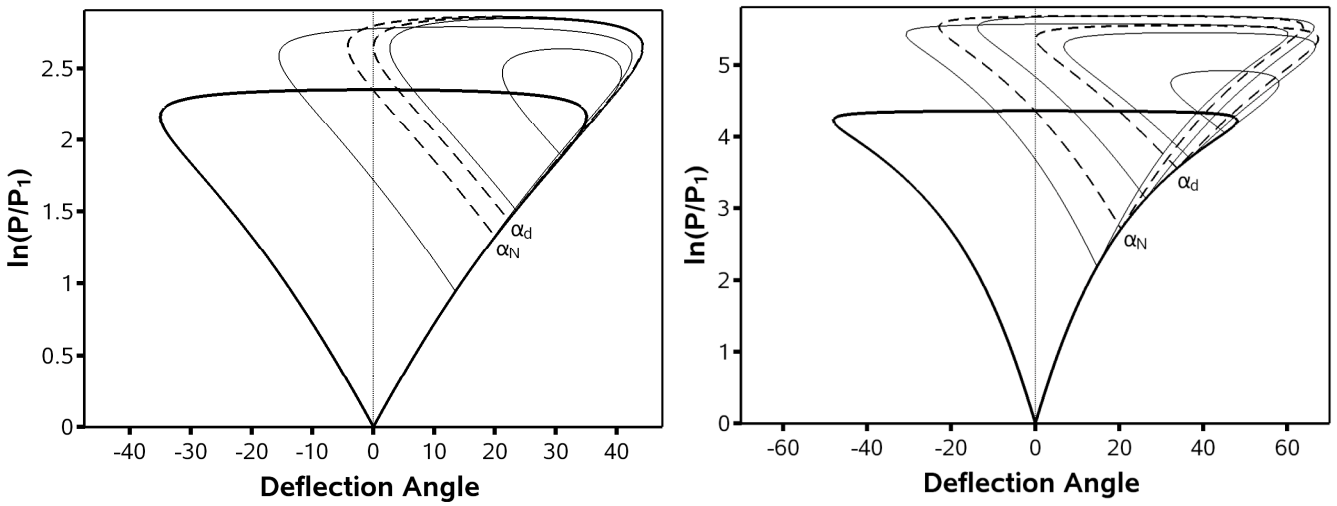

Figure 3. Deflection-pressure diagrams for incident and reflected shock-waves. Inflow Mach number 3 (left) and 8 (right), γ=1.4. Pressure-deflection diagrams for critical values of the incident shock-wave angle are given by dashed lines.

the inflow conditions. This normal shock pressure occurs at $\alpha = \pi/2$ and $\theta = 0$ on the incident shock-wave deflection diagram. For values of α less than α_N, a regular reflection will always occur. The second critical value, labeled α_d, is where the maximum deflection angle of the reflected shock-wave is exactly equal to the deflection angle of the first shock-wave. For α greater than α_d, a Mach reflection will always occur. The region between the two critical values, where $\alpha_N < \alpha < \alpha_d$, is known as the dual-solution-domain (DSD), either a regular reflection or a Mach reflection can exist in the DSD. In general, as the Mach number is increased, the difference between α_N and α_d also increases.

The purpose of this report is to investigate how these critical values for α vary at high Mach numbers where variable thermal properties and dissociation become important. For perfect gases, the critical α's are only a function of upstream Mach number and specific heat ratio. This allows the expressions for determining these values to be simplified dramatically. However, because we do not make the assumption of perfects gases, we need to use iterative techniques in order to determine the correct values for α_N and α_d, using the criteria mentioned previously to determine the critical values. For α_N, this is:

$$P_3\left(\alpha_N, \mathbf{C}_{(1)}\right) - P_n\left(\mathbf{C}_{(1)}\right) = 0 \tag{10}$$

where $P_3\left(\alpha, \mathbf{C}_{(1)}\right)$ is the pressure at station (3) in Figure 1, as a function of the incident shock-wave angle and upstream conditions represented by $\mathbf{C}_{(1)}$. $P_n\left(\mathbf{C}_{(1)}\right)$ is the normal shock-wave pressure jump using the conditions at station (1) upstream of the incident shock-wave. The Mach reflection limit, α_d, is solved by

$$\theta\left(\alpha_d, \mathbf{C}_{(1)}\right) - \theta_{max}\left(\mathbf{C}_{(2)}\right) = 0 \ . \tag{11}$$

The first set of solutions for α_N and α_d are shown in Figure 4. This solution was done for a perfect gas with $\gamma = 1.4$, using the method developed for gases with variable specific heats and possible reactions. The results are compared with Khotyanovsky *et al* [2], and shows that the methods for determining α_N and α_d can reproduce previous results for perfect gases. Since our interest is in the high Mach number range, the Mach number range below 3 was not investigated for this report. Their results were limited to Mach numbers below 6.5. Results for this paper examine critical incident shock-wave angles for Mach numbers in the range of 3.0 all the way to 18.0, to correspond to the large range of conditions seen with blast waves.

Figure 5 shows results for α_N and α_d for perfect gases, where γ varies from 1.2 to 1.6. For comparison, we also compute the curve for curve-fit air properties on the same plot. Although for such a wide range of Mach numbers, we expect temperatures to be high enough to require variable properties for accuracy, the trends that we see for the perfect gas cases are instructive. In this plot, we see that as γ increases, α_N tends to increase and α_d tends to decrease, creating a smaller dual-solution-domain region. The value for γ has a larger effect on the value of α_d than α_N. To relate this to real gases, note that as the temperature rises, the value for C_p generally increases, which will shift the value towards a lower γ. This is seen in Figure 5 for air with variable properties, which has a value of 1.4 at low temperatures, but will increase as the temperature rises. For detonation and combustion products, the value for γ tends to be lower than 1.4 even at low temperatures, due to the larger heat capacity of combustion products. Therefore we expect the detonation results to follow the lower γ curves rather than the higher γ curves. The final interesting result from this figure is how the variable properties curves vary from the perfect gas $\gamma = 1.4$ curves. There is very little difference for α_N, even in the high Mach number limit. There is, however, more variation for the α_d values. This is not surprising, since the larger incident angles result in much larger temperature jumps across the shock, and would thus have a comparatively larger change in γ.

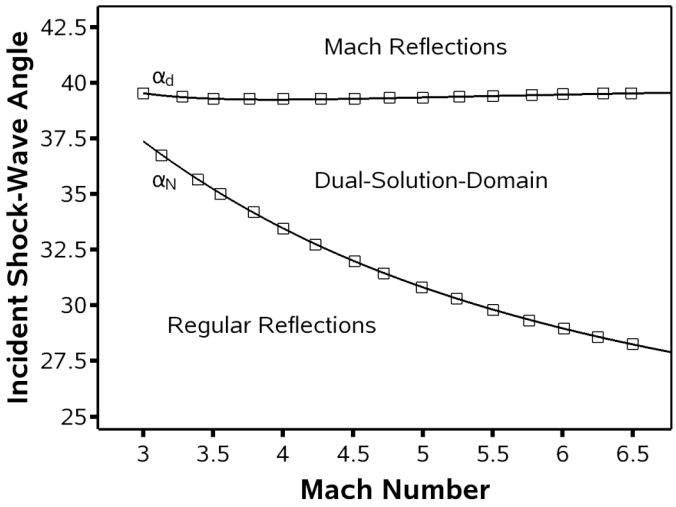

Figure 4. Critical values for incident shock-wave angle for a perfect gas, γ=1.4. Symbols represent data from Khotyanovsky et al [2].

The second main result, shown in Figure 6, examines the critical values for incident shock-wave angle for different combustion type models. For comparison, we have placed the variable properties, air curves on this figure as well. For the detonation products, we use an approximation to the products found in Volk and Schedlbauer [3].

Species	***Mole-fraction***	***Specific heat ratio at 300 K***
Carbon Monoxide (CO)	0.174	1.400
Carbon Dioxide (CO2)	0.100	1.289
Nitrogen (N2)	0.136	1.400
Steam (H2O)	0.198	1.327
Hydrogen (H2)	0.034	1.409
Carbon graphite (C)	0.359	1.000

Each of the species is curve-fit from 200 K to 6000 K. Above 6000 K, we could not find curve-fits for some of the species (H2O and C), and instead extended the specific heat as a constant above 6000 K. This will effect only the high Mach number range of α_d calculation, about Mach 13.2. Below this, and for all of the values for α_N, the temperature is within the 6000 K range.

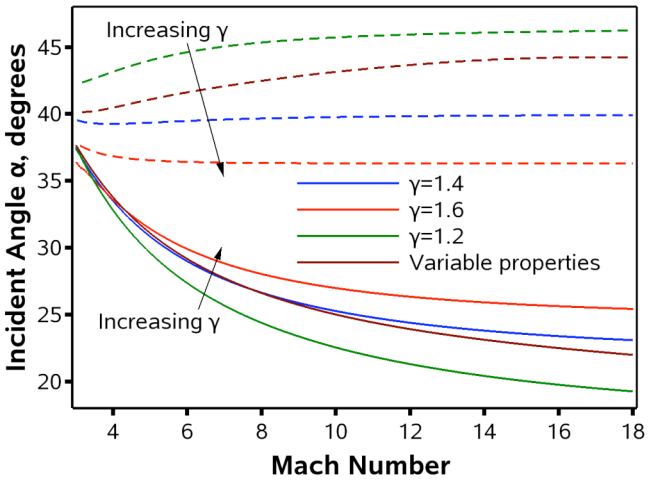

Figure 5. Critical values for incident shock-wave angle for perfect gases and air with variable properties. α_N is represented as a solid line, and α_d as a dashed line.

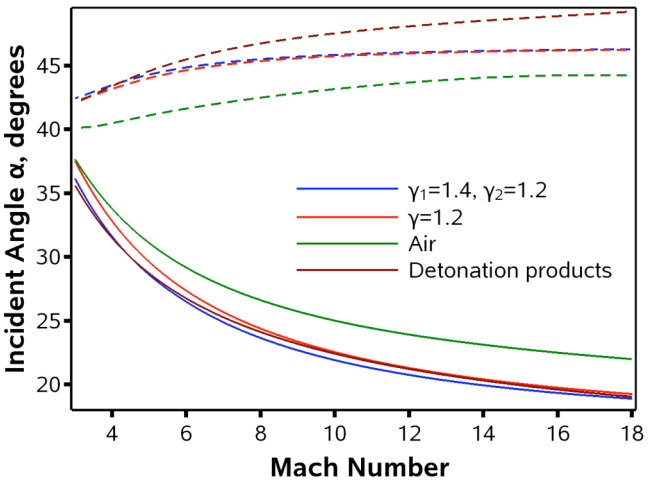

Figure 6. Critical values for incident shock-wave angle for air and detonation products using variable properties. For comparison, two perfect gas cases are also presented.

With this formulation, we also have the ability to examine three different perfect gases at stations (1), (2), and (3) in Figure 1, as well as temperature-dependent variable properties. Thus, at each station, we can have a different value for γ. This could either represent an increase in specific heats due to higher temperatures after the incident shock wave, or it could also represent different compositions due to chemical reactions. In this case, we look at a case where the γ varies from 1.4 in front of the incident shock wave, to 1.2 behind both the incident and reflected shock waves. In Figure 6, we see that the value for α_N appears to be largely dependent on the specific heat ratio after the incident shock wave. The perfect gas solutions for $\gamma = 1.2$ after the incident shock wave both do a remarkable job of reproducing the variable properties result with combustion products. Again, this is most likely due to the minimal temperature rise after shock waves with such low angles of incidence, even at high Mach numbers. More variation is seen with the α_d computation, especially with the combustion products. Again, this is a similar trend as what was seen in Figure 5 with variable properties compared with $\gamma = 1.4$, likely due to increasing specific heats as the temperature increases for the variable property calculations. In all cases seen in Figure 6, the $\gamma = 1.4$ perfect gas solution is considerably different than any of the other approximations, and shows that it is important to consider the effect of different γ's and variable properties.

The final result that we present is shown in Figures 7 and 8. In these plots, we compare a perfect gas with $\gamma = 1.4$, frozen (non-reacting) air with variable properties, and air with equilibrium reactions and variable properties. We show both the critical shock wave angles as Mach number increases, and also the temperature found behind the reflected shock wave, which represents the highest temperature in the system. For the air with equilibrium reactions, we consider the species N2, O2, N, O, and NO as the main constituents. Results show again that α_N has only minor variations when we consider variable properties and equilibrium reactions, but α_d has a much more pronounced variation. Also note that the value for α_d increases as we consider equilibrium reactions. Intuitively, we might think that the value should actually decrease, since the lower temperatures and more monatomic nature of the gas suggests a higher value for γ. This, however, is countered by the dissociation reactions extracting heat from the shocked gases, which tends to shift the value for α_d upwards. Examining Figure 8, we can see the significance of the heat extraction, as the temperature is reduced from 12,674 K to 7458 K due to the dissociation of the molecules. Since dissociation had only a minor effect on the value for α_N with air, we have decided not to do equilibrium reactions for the detonation products.

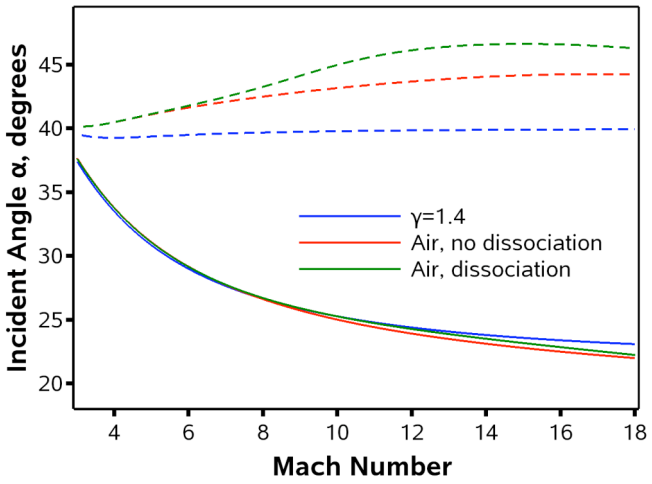

Figure 7. Critical values for incident shock wave angle for air with variable properties, and with and without dissociation.

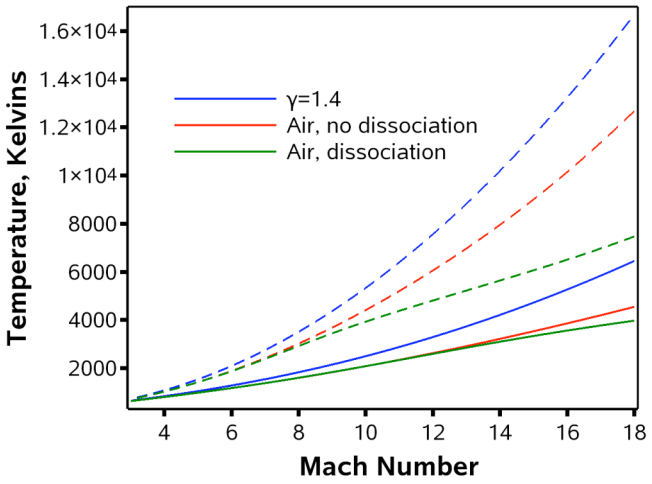

Figure 8. Temperature after the reflected shock at the critical values α_d (dashed) and α_N (solid).

This would prove much more difficult due to the range of possible species and the presence of solid graphite within the flow.

Conclusions

This short report has described calculations performed to determine the critical values for the shock wave angle α_N and α_d for Mach numbers up to 18, for both air and detonation products. We have found that both critical values are very sensitive to the specific heat ratio after the incident shock wave. For perfect gases, as γ decreases, the value for α_d increases and the value for α_N decreases, thus increasing significantly the dual-solution-domain where both regular and Mach reflections can exist. For α_N, the results were fairly insensitive to variable specific heats even at very high Mach number, and adequate approximations can be made without considering a variable specific heat, although careful attention should be made to the selection of γ. α_d showed a much greater sensitivity to variable properties, and both variable properties and equilibrium reactions should be considered when computing this critical value even at relatively low Mach numbers. Although the value for α_N is fairly insensitive to variable properties, the temperature behind the reflected shock does vary significantly for variable specific heats. If this parameter is important for the specific application under investigation than variable specific heats should be considered. Equilibrium chemistry was not included with the detonation products because our main interest was determining good values for α_N at very high Mach numbers. The complete iterative equations, as well as the curve-fits used for the specific heat, enthalpy, and entropy computations, are given in the Appendix.

References

1. Hornung, H. "Regular and Mach reflection of shock waves." *Ann. Rev. Fluid Mech.* **18**: 33-58, 1986.
2. Khotyanovsky, D.V., Kudryavtsev, A.N., and Ivanov, M.S. "Effects of a single-pulse energy deposition on steady shock wave reflection." *Shock Waves* **15**: 353-362, 2006.
3. Volk, F. and Schedlbauer, F. "Analysis of post detonation products of different explosive charges." *Propellants, Explosives, Pyrotechnics* 24: 182-188, 1999.
4. Gordon, S. and McBride, B.J. "Computer Program for Calculation of Complex Chemical Equilibrium Compositions and Applications." NASA Reference Publication 1311, 1994.

Appendix A. Solution Procedure for Real Gases

To compute properties across an oblique shock for variable specific heat properties, we must use an iterative algorithm. The algorithm is based on the conserved variables across a shock. For an oblique shock where the normal velocity across the shock is and the tangential component is w, the mass, momentum, and energy equations can be reduced to:

We can rearrange these equations in terms of an iterative variable $R = \rho_1 / \rho_2$. This variable will always be less than 1. The momentum, energy, and continuity equations can be rewritten:

$$p_2 = p_1 + \rho_1 u_1^2 (1 - R) \tag{12}$$

$$h_2 = h_1 + \frac{u_1^2}{2}\left(1 - R^2\right) \tag{13}$$

$$u_2 = u_1 R \tag{14}$$

The iterative procedure employed is relatively simple. First, an initial value for R is guessed. There are several ways to get a good guess for R, but what we've found is robust convergence is fairly independent of this initial guess. Therefore, we typically assume an initial value of $R = 0.1$. The iterative process is then:

1. Solve equation (12) for p_2.
2. Solve equation (13) for h_2.
3. Calculate ρ_2 from equation (7).
4. Calculate new $R^{n+1} = \rho_1 / \rho_2$.
5. Check for convergence of R^{n+1}. If not converged, go back to step 1.
6. Calculate u_2 from equation (14).

We converge $\left(R^{n+1} - R^n\right) / R^{n+1}$ down to 1×10^{-8}.

For non-reacting shock waves (where no dissociation occurs), equation (7) is fairly simple to compute. For reacting shock waves, the situation can be more complex. If we know the composition of the products, such as assuming a fuel gas is completely consumed to products, then we use a similar iterative solution as above. If, however, we are interested in equilibrium concentrations (for instance, if we are assuming dissociation of air species), then we must solve an iterative set of equations for the composition and temperature, holding enthalpy and pressure constant.

In both cases, once temperature and compositions are found, we use the ideal gas law to compute the density:

$$\rho = \frac{p}{RT} \sum_{i=1}^{NS} X_i M_i \Big/ \sum_{i=1}^{NG} X_i \tag{15}$$

where NS is the total number of species, and NG is the number of gas species. If all species are gaseous, than $\sum X_i = 1$.

Appendix B. Thermal Properties Calculation

Thermal properties for the gas mixture is obtained through curve-fits for the enthalpy, entropy, and specific heat. These properties take the general form for species j:

$$\overline{C}_{p,j}^{o} = \sum\left(c_{j,i}T^{m_i}\right) \tag{16}$$

For the CEA database [4], each species specific heat is modeled by three 7th-order polynomials in the form of Eqn. 16, with temperature ranges from 200-1000 K, from 1000-6000 K, and 6000-20,000 K. The value for m_i varies from -2 to 5. Enthalpy and entropy values are obtained by using the relations:

$$\overline{h}_j^o(T) = \int \overline{C}_{p,j}(\tau)d\tau + c_{j,N+1} \tag{17}$$

$$\overline{s}_j^o(T) = \int \frac{\overline{C}_{p,j}(\tau)}{\tau} d\tau + c_{j,N+2} \tag{18}$$

For each curve-fit, enthalpy and entropy at any temperature is specified with the above definitions and a constant representing the enthalpy and entropy of formation. For a mixture, the specific enthalpy and entropy (molar-basis) are simply summations of species enthalpies multiplied by their mole-fractions, i.e.,

$$\overline{h}(T) = \sum X_j \overline{h}_j^o(T) \tag{19}$$

For shock-wave problems, we typically know the specific enthalpy and composition, and need to solve for temperature T. In these cases, we use an iterative Newton-Rhapson method to converge on the appropriate temperature, which works well due to the smoothness of the specific heat curves. The bar above the variables indicate that these are mole based properties; to convert to mass based properties (that are used in the conservation equations) we divide by the molecular weight. For species in the CEA database, the $\overline{C}_{p,j}^{o}$ is fitted using a 7th-order polynomial, as shown below:

$$\overline{C}_{p,j}^{o}(T) = \frac{c_{j,1}}{T^2} + \frac{c_{j,2}}{T} + c_{j,3} + c_{j,4}T + c_{j,5}T^2 + c_{j,6}T^3 + c_{j,7}T^4 \tag{20}$$

$$\overline{h}_j^o(T) = -\frac{c_{j,1}}{T} + c_{j,2}\ln T + c_{j,3}T + c_{j,4}\frac{T^2}{2} + c_{j,5}\frac{T^3}{3} + c_{j,6}\frac{T^4}{4} + c_{j,7}\frac{T^5}{5} + c_{j,8} \tag{21}$$

$$\overline{s}_j^o(T) = -\frac{c_{j,1}}{2T^2} - \frac{c_{j,2}}{T} + c_{j,3}\ln T + c_{j,4}T + c_{j,5}\frac{T^2}{2} + c_{j,6}\frac{T^3}{3} + c_{j,7}\frac{T^4}{4} + c_{j,9} \tag{22}$$

Appendix C. Chemical Equilibrium

The equilibrium calculation is discussed in detail in NASA Reference Publication 1311 [4]. We only summarize the equations here for completeness. We do not use the CEA program directly, but have instead re-implemented the algorithm to better incorporate it into the current solution procedure. The equilibrium calculation minimizes the Gibbs free energy for the system. This minimization is done by solving the system $\delta G = 0$, and using a Newton-Rhapson iterative scheme to converge the system. By applying the constraint that the element number must be conserved, we get a set of reduced Gibbs iterative equations assuming no condensed phases:

$$\sum_{i=1}^{NE}\sum_{j=1}^{NG} a_{kj}a_{ij}n_j\pi_i + \left(\sum_{j=1}^{NG} a_{kj}n_j\right)\Delta\ln n + \left(\sum_{j=1}^{NG}\frac{a_{kj}n_j\bar{h}_j^o}{RT}\right)\Delta\ln T = b_{k,o} - b_k + \sum_{j=1}^{NG}\frac{a_{kj}n_j\mu_j}{RT} \tag{23}$$

$$\sum_{i=1}^{NE}\sum_{j=1}^{NG} a_{ij}n_j\pi_i + \left(\sum_{j=1}^{NG} n_j - n\right)\Delta\ln n + \left(\sum_{j=1}^{NG}\frac{n_j\bar{h}_j^o}{RT}\right)\Delta\ln T = n - \sum_{j=1}^{NG} n_j + \sum_{j=1}^{NG}\frac{n_j\mu_j}{RT} \tag{24}$$

$$\begin{aligned}&\sum_{i=1}^{NE}\left(\sum_{j=1}^{NG}\frac{a_{ij}n_j\bar{h}_j^o}{RT}\right)\pi_i + \left(\sum_{j=1}^{NG}\frac{n_j\bar{h}_j^o}{RT}\right)\Delta\ln n + \\ &\left[\sum_{j=1}^{NG}\frac{n_j\bar{C}_{p,j}^o}{R} + \sum_{j=1}^{NG}\frac{n_j\left(\bar{h}_j^o\right)^2}{R^2T^2}\right]\Delta\ln T = \frac{h_o - h}{RT} + \sum_{j=1}^{NG}\frac{n_j\bar{h}_j^o\mu_j}{R^2T^2}\end{aligned} \tag{25}$$

NE is the number of elements, n_j is defined as the number of moles of species j per kg mixture. a_{ij} are the number of atoms of element i in species j. $b_i = \sum a_{ij}n_j$. $b_{i,o}$ indicates the assigned number of moles of atom i per kg mixture. n is the moles of gas per kg of mixture, $n = \sum n_j$. μ_j is the chemical potential of species j, defined below for gases:

$$\mu_j = \bar{h}_j^o - \bar{s}_j^o T + RT\ln\left(n_j/n\right) + RT\ln\left(p/p^o\right) \tag{26}$$

where p^o is the standard-state pressure. π_i is related the Lagrange multiplier that is needed for the solution method, where $\pi_i = -\lambda_i/RT$.

The iteration variables for Eqns (23-25) are π_i, $\Delta\ln n$, and $\Delta\ln T$. This gives us $NE+2$ equations to solve simultaneously. We use the LAPACK routines to solve this system of equations. The gaseous species concentrations are then:

$$\Delta\ln n_j = -\frac{\mu_j}{RT} + \sum_{i=1}^{NE} a_{ij}\pi_i + \Delta\ln n + \frac{\bar{h}_j^o}{RT}\Delta\ln T \tag{27}$$

We then use these values to iterate on the composition and temperature:

$$\ln n_j^{(m+1)} = \ln n_j^{(m)} + \lambda^{(m)}\left(\Delta\ln n_j\right)^{(m)} \tag{28}$$

$$\ln n^{(m+1)} = \ln n^{(m)} + \lambda^{(m)}\left(\Delta\ln n\right)^{(m)} \tag{29}$$

$$\ln T^{(m+1)} = \ln T^{(m)} + \lambda^{(m)}\left(\Delta\ln T\right)^{(m)} \tag{30}$$

where $\lambda^{(m)}$ is a relaxation factor to ensure that the corrections remain constrained for the mth iteration. Reference 4 gives a detailed description of how $\lambda^{(m)}$ is chosen. The convergence criteria is:

$$\frac{n_j \left| \Delta \ln n_j \right|}{n_{tot}} < 0.5 \times 10^{-5} \tag{31}$$

$$\frac{n \left| \Delta \ln n \right|}{n_{tot}} < 0.5 \times 10^{-5} \tag{32}$$

$$\frac{\left| b_{i,o} - \sum_{j=1}^{NS} a_{ij} n_j \right|}{\left(b_{i,o} \right)_{max}} < 10^{-6} \tag{33}$$

where $n_{tot} = \sum n_j$ and $\left(b_{i,o} \right)_{max}$ refers to the chemical element with the largest value of $b_{i,o}$.

An initial guess for the composition is provided by the user, along with an initial guess for the temperature. For the shock wave calculations presented in this report, we assume no dissociation to obtain an initial guess for the composition and temperature. Convergence usually occurs within 18 to 19 iterations for the air equilibrium species. This convergence is clearly dependent on the problem, however, and the number of species and elements considered in the system.